Optics Letters

Low-loss fs-laser-written surface waveguide lasers at >2 μm in monoclinic Tm^{3+}:$MgWO_4$

Esrom Kifle,[1] Pavel Loiko,[2] Javier Rodríguez Vázquez de Aldana,[3] Carolina Romero,[3] Víctor Llamas,[1,4] Josep Maria Serres,[1,4] Magdalena Aguiló,[1] Francesc Díaz,[1] Lizhen Zhang,[5] Zhoubin Lin,[5] Haifeng Lin,[5] Ge Zhang,[5] Viktor Zakharov,[6] Andrey Veniaminov,[6] Valentin Petrov,[7] Uwe Griebner,[7] Xavier Mateos,[1,*] Li Wang,[7] and Weidong Chen[5,7]

[1]Universitat Rovira i Virgili (URV), Física i Cristal·lografia de Materials i Nanomaterials (FiCMA-FiCNA)-EMaS, Marcel.li Domingo 1, 43007 Tarragona, Spain
[2]Centre de Recherche sur les Ions, les Matériaux et la Photonique (CIMAP), UMR 6252 CEA-CNRS-ENSICAEN, Université de Caen Normandie, 6 Boulevard du Maréchal Juin, 14050 Caen Cedex 4, France
[3]Aplicaciones del Láser y Fotónica, University of Salamanca, 37008 Salamanca, Spain
[4]Eurecat, Centre Tecnològic de Catalunya, Unitat Advanced Manufacturing Systems (AMS), Campus Sescelades, 43007 Tarragona, Spain
[5]Key Laboratory of Optoelectronic Materials Chemistry and Physics, Fujian Institute of Research on the Structure of Matter, Chinese Academy of Sciences, Fuzhou, 350002 Fujian, China
[6]ITMO University, 49 Kronverkskiy Pr., 197101 St. Petersburg, Russia
[7]Max-Born-Institute for Nonlinear Optics and Short Pulse Spectroscopy, 2A Max-Born-Str., 12489 Berlin, Germany
*Corresponding author: xavier.mateos@urv.cat

Received 23 April 2020; revised 13 June 2020; accepted 14 June 2020; posted 15 June 2020 (Doc. ID 395811); published 14 July 2020

Surface channel waveguides (WGs) based on a half-ring (40–60-μm-diameter) depressed-index cladding (type III) geometry are fabricated in monoclinic Tm^{3+}:$MgWO_4$ by femtosecond (fs) laser writing at a repetition rate of 1 kHz. The WGs are characterized by confocal laser microscopy and μ-Raman spectroscopy. A Tm^{3+}:$MgWO_4$ WG laser generates 320 mW at ~2.02 μm with a slope efficiency of 64.4%. The WG emits a transverse single-mode and linear polarization ($E||N_m$). A remarkable low loss of < 0.1 dB/cm is measured for the WG. Vibronic laser emission at ~2.08 μm is also achieved.

https://doi.org/10.1364/OL.395811

Magnesium monotungstate ($MgWO_4$) has been recognized recently as an excellent host material for doping with trivalent thulium ions (Tm^{3+}) [1,2]. It belongs to the monoclinic crystal class (sp. gr. $C_{2h}^4 - P2/c$, wolframite, [Fe, Mn]WO_4, type structure) [3] and shows a single crystallographic site for Tm^{3+} ions (the Mg^{2+} one, symmetry: C_2). Charge compensation for the heterovalent doping is provided by univalent alkali-metal cations (e.g., Na^+) in the flux [4]. $MgWO_4$ exhibits good thermo-mechanical properties, such as high thermal conductivity $\langle\kappa\rangle = 8.7\ Wm^{-1}\ K^{-1}$ [5] and low anisotropy of the thermal expansion, $\alpha_a = 11.22$, $\alpha_b = 8.09$, and $\alpha_c = 8.77$ [$10^{-6}\ K^{-1}$] [4], leading to promising power scaling capabilities.

For Tm^{3+} ions (electronic configuration: [Xe]$4f^{12}$), $MgWO_4$ shows attractive spectroscopic properties, i.e., intense and broad emission bands for the $^3F_4 \rightarrow {}^3H_6$ transition with polarized light and large Stark splitting of the ground state, $\Delta E(^3H_6) = 633\ cm^{-1}$ [6]. Thus, the broad polarized emission bands of Tm^{3+}:$MgWO_4$ extend well above 2 μm, avoiding the structured water vapor atmospheric absorption. The latter is a key issue for the generation of femtosecond (fs) pulses in mode-locked (ML) lasers in the 2 μm spectral range [7]. It was recently confirmed by a graphene ML Tm^{3+}:$MgWO_4$ laser, which generated 86 fs pulses at a wavelength of 2017 nm (bandwidth: 53 nm) at a repetition rate of 87 MHz [2]. Furthermore, continuous wavelength tuning was achieved from 1897 to 2062 nm [2]. As $MgWO_4$ is an efficient Raman-active material, laser emission at even longer wavelengths (up to 2093 nm) was realized due to the electron–phonon coupling [6]. A continuous-wave (CW) Tm^{3+}:$MgWO_4$ laser generated 3.09 W at 2022–2034 nm with a slope efficiency as high as 50% [1].

Due to its attractive thermal and spectroscopic properties, Tm^{3+}:$MgWO_4$ is also promising for ML waveguide (WG) lasers above 2 μm. While Tm^{3+}-doped monoclinic double-tungstate (MDT) bulk crystals have been widely explored to this aim [8], WG laser operation has never been demonstrated with monoclinic divalent-metal monotungstates. In the present work, we demonstrate the first, to the best of our knowledge, Tm^{3+}:$MgWO_4$ WG laser featuring low passive losses and high laser efficiency, as a first step towards high-repetition-rate [gigahertz (GHz)-range)] ML WG lasers [9].

As a fabrication method, we selected fs direct laser writing (fs-DLW). This method is based on focusing a fs laser beam inside a small volume [few (μm^3)] within a transparent material resulting in partial amorphization of the damaged area

leading to a permanent refractive-index variation ($\Delta n > 0$ or $\Delta n < 0$) [10]. The advantages of fs-DLW are short interaction time and high-precision, single-step procedure, suitability for various materials *including* anisotropic crystals, variable WG geometries, and moderate to low propagation losses. Efficient fs-DLW thulium WG lasers have been demonstrated [11,12]. Lancaster *et al.* reported on a buried channel WG laser inscribed in a Tm^{3+}:ZBLAN glass delivering 205 mW at ~ 1.89 μm with a slope efficiency η of 67% and low passive losses δ_{loss} of 0.4 ± 0.2 dB/cm [11]. Kifle *et al.* demonstrated a surface WG laser in a Tm^{3+}:$KLu(WO_4)_2$ crystal generating 171 mW at ~ 1.85 μm with $\eta = 38\%$ and $\delta_{loss} = 0.7 \pm 0.3$ dB/cm [12].

The Tm^{3+}:$MgWO_4$ crystal was grown by the top-seeded solution growth (TSSG) method using Na_2WO_4 as a solvent [13]. The Tm^{3+} doping level was 0.89 at.% ($N_{Tm} = 1.41 \times 10^{20}$ cm^{-3}). A rectangular sample with dimensions $1.86(N_g) \times 3.96(N_m) \times 3.05(N_p)$ was cut and polished along the optical indicatrix frame of this biaxial crystal [6]. The DLW was performed using 120 fs pulses with a central wavelength of 795 nm from a Ti:Sapphire regenerative amplifier at a repetition rate of 1 kHz. A small portion of the pulse energy (86 nJ, measured after the focusing optics) was employed with polarization $\boldsymbol{E}||N_m$. The fs radiation was focused into the crystal along the N_g axis through the top surface using a 40× microscope objective (N.A. = 0.65). The sample was translated at a speed of 400 μm/s along the N_p axis producing damage tracks.

Surface channel WGs with a half-ring depressed-index cladding ($\Delta n > 0$, classified as type III microstructures [10]) were produced. Their geometry was revealed using confocal laser microscopy, Fig. 1(a). The diameter of the cladding was 40, 50, or 60 μm. The axis of the WG was located at 20–30 μm beneath the top surface. Except for the damage tracks, no cracks in the writing areas or in the bulk volume were observed. The damage tracks passed continuously through the whole length of the 3.05 mm long sample (along the N_p axis), Fig. 1(b). The study of the sample in crossed polarizers (P and A) revealed bright areas localized at the damage tracks, indicating a local alteration of the size and orientation of the optical indicatrix, Fig. 1(c). The damage tracks reached the top surface of the WGs, Fig. 1(d), thus producing a shallow ablation groove at the external tracks.

Raman spectroscopy is a sensitive tool to study the structure alteration at the μ scale [14]. The polarized Raman spectrum of the Tm^{3+}:$MgWO_4$ crystal for the $p(\text{mm})\bar{p}$ geometry (Porto's notations) is shown in Fig. 2(a). The most intense Raman band denoted as $\nu_1(A_{1g})$ is observed at ~ 916 cm^{-1} and assigned to symmetric stretching W–O vibrations in the [WO_6] octahedra [13]. The peak intensity, width (FWHM), μ and position were monitored over the sample end-facet resulting in μ-Raman maps, Figs. 2(c) and 2(d). In the damaged regions, a drop of intensity, broadening of the band, and its shift to longer frequencies are observed, indicating a reduction of crystallinity (a partial amorphization). The crystalline quality of the core is well preserved, as manifested by the almost unchanged Raman response with respect to the bulk regions.

In Tm^{3+}:$MgWO_4$, the maximum absorption cross section, σ_{abs}, for the $^3H_6 \rightarrow {}^3H_4$ pump transition is 1.43×10^{-20} cm^2 at 800.3 nm, Fig. 3(a). The peak stimulated-emission (SE) cross section, σ_{SE}, at wavelengths > 2 μm, where the laser operation is

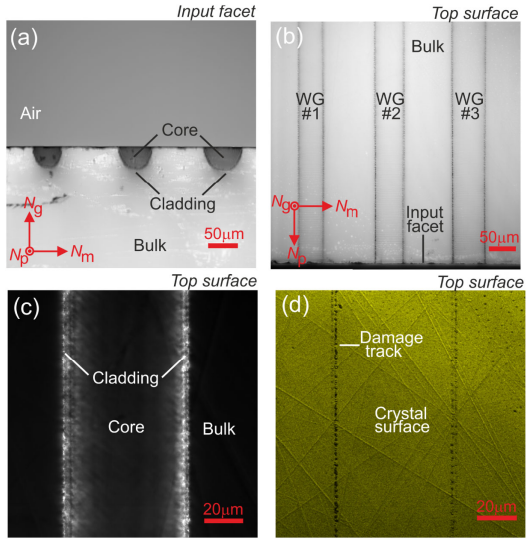

Fig. 1. Confocal microscopy study of fs-DLW surface channel WGs in Tm^{3+}:$MgWO_4$: (a) end-facet view, transmission mode, polarized light ($P||N_g$); (b) and (c) top surface view, transmission mode: (b) a general view in polarized light ($P||N_p$); (c) a close look at the 60 μm WG in crossed polarizers ($P||N_p$, $A||N_m$); (d) the same area as in (c) in reflection mode. λ = 405 nm. P, polarizer; A, analyzer.

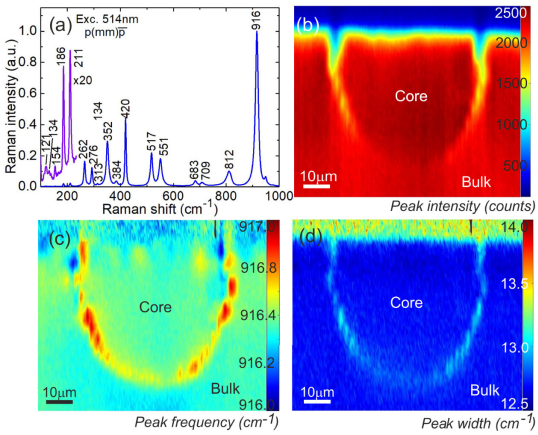

Fig. 2. Micro-Raman mapping of the fs-DLW surface channel WG (size: 50 μm) in Tm^{3+}:$MgWO_4$: (a) polarized Raman spectrum for the $p(\text{mm})\bar{p}$ geometry, numbers denote the Raman frequencies in cm^{-1}, $\lambda_{exc} = 514$ nm; (b)–(d) maps of the crystal end-facet representing the variation of (b) peak Raman intensity, (c) peak frequency, and (d) peak width (FWHM) for the ~ 916 cm^{-1} Raman band.

expected, is 0.85×10^{-20} cm^2 at 2015 nm, Fig. 3(b). Both values are specified for $\boldsymbol{E}||N_m$. The upper laser-level ($^3F_4$) lifetime is 1.93 ms [13].

The laser cavity comprised a flat pump mirror coated for high transmission (HT) ($T = 96\%$) at 0.80 μm and for high reflection (HR) at 1.80–2.06 μm and a set of flat output couplers (OCs) having a transmission $T_{OC} = 1.5 - 30\%$ at the laser wavelength. We also used a special bandpass OC coated for HT at < 2 μm and providing $T_{OC} = 1.6\%$ at > 2.05 μm. All the OCs provided HR at ~ 0.80 μm, so the WG was pumped in a double pass. The crystal was mounted on a passively cooled BK7 glass block and placed between the cavity mirrors without

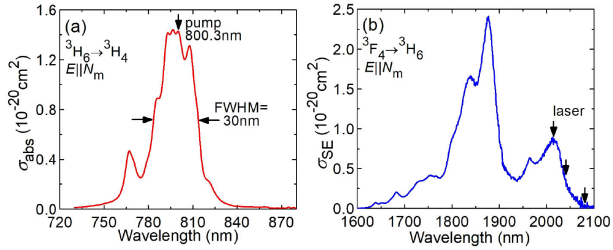

Fig. 3. Spectroscopy of Tm^{3+} ions in monoclinic $MgWO_4$: (a) absorption cross section, σ_{abs}, for the $^3H_6 \rightarrow {}^3H_4$ transition, and (b) stimulated-emission (SE) cross section, σ_{SE}, for the $^3F_4 \rightarrow {}^3H_6$ transition. The light polarization is $\boldsymbol{E}||N_m$. The vertical *arrows* in (a), (b) indicate the pump and emission wavelengths for the WG laser, respectively.

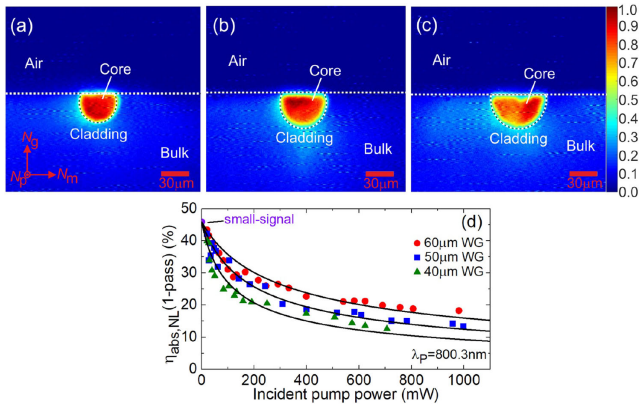

Fig. 4. (a)–(c) Pump modes at the output facet of the fs-DLW WGs in Tm^{3+}:$MgWO_4$: the WG cladding diameters are (a) 40 μm, (b) 50 μm, and (c) 60 μm. *White dashed lines* indicate the WG cladding and the air/crystal interfaces; they are drawn as guides for the eye. The pump polarization ($\boldsymbol{E}||N_m$) is horizontal. (d) Measured single-pass pump absorption in all the WGs under non-lasing conditions, $\eta_{abs,NL}$: *symbols*, experimental data; *curve*, simulation with a rate-equation model using the spectroscopic data from [13]. The pump wavelength is 800.3 nm.

index-matching among them. The mirrors were gently pressed towards the WG endfaces, resulting in a geometrical cavity length of ~ 3.1 mm.

The pump power from a CW Ti:Sapphire laser was up to ~ 2 W at 800.3 nm ($M^2 \approx 1$). The pump, polarized with $\boldsymbol{E}||N_m$ (in the crystal), was focused using a 10× microscope objective (N.A. = 0.28, $f = 20$ mm, $T = 75\%$ at 0.80 μm) to a spot with a diameter of 25 ± 5 μm. The pump coupling efficiency, η_{coupl}, was estimated to be 88.4 ± 1% from pump-transmission measurements at 830 nm. The pump is confined in the slightly D-shaped cladding profile; no leakage into the bulk was detected, Fig. 4(a). The single-pass pump absorption under non-lasing conditions, $\eta_{abs,NL}$, determined at 800.3 nm by the end-fire method, gradually decreased with the incident pump power P_{inc} due to the ground-state bleaching. This effect was enhanced for smaller cladding diameters. The absorbed pump power P_{abs} was determined from $\eta_{abs,NL}$ at the threshold power for each OC, accounting for double-pass pumping.

The input–output characteristics for the 60 μm WG are shown in Fig. 5(a). Exceptionally for the best-performing

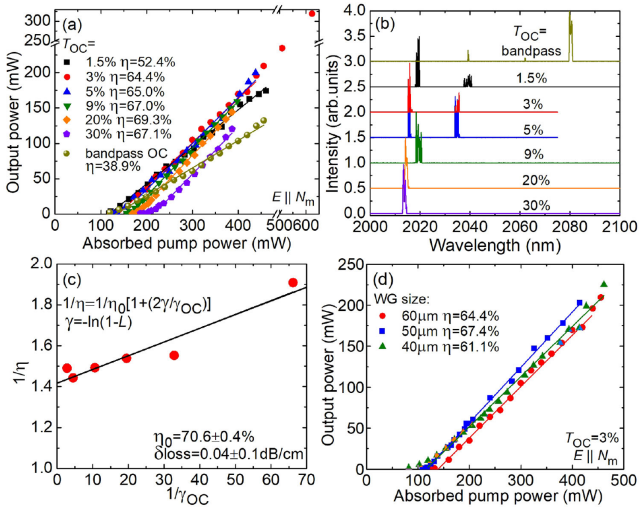

Fig. 5. (a)–(c) Fs-DLW Tm^{3+}:$MgWO_4$ surface channel WG (60 μm) laser: (a) input–output dependences, η, slope efficiency; (b) laser emission spectra measured at the maximum P_{abs}. (c) Caird analysis: the plot of the inverse of the slope efficiency, $1/\eta$, versus inverse of the output coupling loss, $1/\gamma_{OC}$, $\gamma_{OC} = -\ln(1 - T_{OC})$. (d) Comparison of the output performance of WGs with cladding diameters of 40–60 μm: η, slope efficiency; $T_{OC} = 3\%$. The laser polarization is $\boldsymbol{E}||N_m$.

$T_{OC} = 3\%$, we removed the optical elements placed to attenuate P_{inc}, resulting in higher pump power. The laser generated 320 mW at ~ 2015 and 2036 nm with a slope efficiency η of 64.4% (versus P_{abs}). The laser threshold was at $P_{abs} = 126$ mW, and the optical-to-optical efficiency at the maximum pump level was 24.7% (versus P_{inc}). The total pump absorption (in two passes) was 48.1%. The laser slope efficiency slightly increased with the output coupling, reaching $\eta = 69.3\%$ for $T_{OC} = 20\%$. The laser threshold decreased for smaller T_{OC}, from 186 mW (30% OC) down to 117 mW (1.5% OC). No thermal roll-over in the output dependences was detected; the power scaling was limited by the available pump.

The polarization of the laser emission was linear ($\boldsymbol{E}||N_m$), naturally selected by the strong anisotropy of the gain in Tm^{3+}:$MgWO_4$. The laser spectra are shown in Fig. 5(b). For small $T_{OC} < 9\%$, the emission occurred at ~ 2.02 and 2.04 μm. For higher output coupling (9-30%), only the short-wavelength emission was supported due to the quasi-three-level nature of the $^3F_4 \rightarrow {}^3H_6$ Tm^{3+} laser scheme, i.e., influenced by reabsorption.

The passive losses in the 60 μm WG were estimated using the Caird analysis [15], Fig. 5(c). The resulting internal slope efficiency was $\eta_0 = 70.6 \pm 0.4\%$ and $\delta_{loss} = 0.04 + 0.1$ dB/cm. This value is well below those reported previously for fs-DLW WGs in Tm^{3+}:ZBLAN glass (0.4 ± 0.2 dB/cm) [11]. Moreover, the passive loss is comparable with the best reports on surface channel (ridge) WGs in Tm^{3+}:MDT single-crystalline films fabricated by liquid phase epitaxy (LPE) and Ar^+ ion beam milling (< 0.11 dB/cm) [16].

We also studied the laser performance employing the band-pass OC, [Figs. 5(a) and 5(b), dark green]. The laser exhibited a low laser threshold of 120 mW and generated 132 mW at ~ 2080 nm with $\eta = 38.9\%$. This wavelength is well beyond the limit for the purely electronic $^3F_4 \rightarrow {}^3H_6$ Tm^{3+} transition

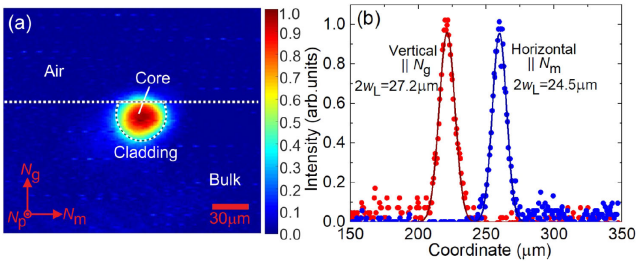

Fig. 6. (a) Spatial near-field laser mode profile of the 40 μm WG fabricated by fs-DLW in Tm^{3+}:$MgWO_4$. $P_{abs} = 0.4$ W, $T_{OC} = 9\%$. The laser polarization is horizontal ($\boldsymbol{E}||N_m$). *White lines* indicate the WG cladding and the air/crystal interfaces; they are drawn as guides for the eye. (b) 1D intensity plots of the intensity profile: *symbols*, experimental points; *curves*, their Gaussian fits.

in $MgWO_4$ (2017 nm, between the Stark sub-levels with the energies 5591 cm^{-1} ($^3F_4$) and 633 cm^{-1} ($^3H_6$) [6]), i.e., the first, to the best of our knowledge, demonstration of a vibronic WG laser. It is assigned to the electron–phonon coupling with the low-frequency Raman modes in $MgWO_4$ [17], Fig. 2(a), such as 121 (A_g), 134, or 154 (both B_g) cm^{-1}.

The performance of the surface WG lasers with different sizes of the cladding (40–60 μm) is compared in Fig. 5(d). The slope efficiency was similar for all the studied guides, while the laser threshold clearly decreased for smaller cladding diameter: it amounted to 108 mW (50 μm WG) and 82 mW (40 μm WG), both for $T_{OC} = 3\%$. The laser polarization for all the WGs was $\boldsymbol{E}||N_m$.

All of the studied WG lasers operated in the fundamental transverse mode. The latter might benefit from additional mode "filtering" provided by the reabsorption (gain-guiding) [18]. An example of the mode for the 40 μm WG is shown in Fig. 6(a). It is well confined within the WG cladding. The one-dimensional (1D) intensity profiles, Fig. 6(b), are well fitted to a Gaussian distribution (goodness of fit: $R^2 > 0.99$), yielding mode diameters $2w_L(||N_g) = 27.2$ μm and $2w_L(||N_m) = 24.5$ μm. The mode ellipticity is weak ($e = 1.11$).

The numerical aperture (N.A.) of the guides was estimated by measuring the divergence of the laser beam θ (half-angle) as N.A. $= \sin\theta$. It was similar along the vertical and horizontal directions, N.A. $= 0.082$ and 0.087 ± 0.005, respectively. Within the approximation of a set-index guide, $\text{N.A.}^2 \approx 2n_{core}\Delta n$, one obtains $\Delta n = n_{cladding} - n_{core}$ of about -1.7×10^{-3} (here, $n_{core} \sim 2.03$ for $\boldsymbol{E}||N_m$ [6]). A similar value was reported for Tm^{3+}:ZBLAN glass ($\Delta n \sim -1.5 \times 10^{-3}$) [11].

To conclude, the monoclinic crystal Tm^{3+}:$MgWO_4$ is promising for highly efficient low-loss (< 0.1 dB/cm) fs-DLW WG lasers at wavelengths above 2 μm, due to its attractive spectroscopic, vibronic, and thermal properties. In the present work, we achieved the highest slope efficiency (69.3%) and output power (320 mW) for any thulium WG laser fabricated by fs-DLW. Furthermore, the first, to the best of our knowledge, "vibronic" Tm WG laser with the longest emission wavelength of 2080 nm for Tm-doped WGs is also demonstrated. The designed photonic μ-structures with a size in the few millimeters range are highly attractive for the generation of ultrashort pulses in compact ML lasers operating at high repetition rates (GHz range), as well as for surface activation, e.g., leading to pulsed operation via evanescent-field coupling.

Funding. Ministerio de Economía y Competitividad (FIS2017-87970-R, MAT2016-75716-C2-1-R (AEI/FEDER, UE)); Agència de Gestió d'Ajuts Universitaris i de Recerca (2017SGR755); Consejería de Educación, Junta de Castilla y León (SA287P18); National Natural Science Foundation of China (51761135115, 61575199, 61850410533, 61875199, 61975208); Ministry of Science and Higher Education of the Russian Federation (Goszadanie 2019-1080); Deutsche Forschungsgemeinschaft (PE 607/14-1).

Acknowledgment. Víctor Llamas is a fellow of Eurecat's "Vicente López" PhD grant program.

Disclosures. The authors declare no conflicts of interest.

REFERENCES

1. P. Loiko, J. M. Serres, X. Mateos, M. Aguiló, F. Díaz, L. Zhang, Z. Lin, H. Lin, G. Zhang, K. Yumashev, V. Petrov, U. Griebner, Y. Wang, S. Y. Choi, F. Rotermund, and W. Chen, Opt. Lett. **42**, 1177 (2017).
2. Y. Wang, W. Chen, M. Mero, L. Zhang, H. Lin, Z. Lin, G. Zhang, F. Rotermund, Y. J. Cho, P. Loiko, X. Mateos, U. Griebner, and V. Petrov, Opt. Lett. **42**, 3076 (2017).
3. V. B. Kravchenko, J. Struct. Chem. **10**, 139 (1969).
4. L. Zhang, P. Loiko, J. M. Serres, E. Kifle, H. Lin, G. Zhang, E. Vilejshikova, E. Dunina, A. Kornienko, L. Fomicheva, U. Griebner, V. Petrov, Z. Lin, W. Chen, K. Subbotin, M. Aguiló, F. Díaz, and X. Mateos, J. Lumin. **213**, 316 (2019).
5. L. Zhang, Y. Huang, S. Sun, F. Yuan, Z. Lin, and G. Wang, J. Lumin. **169**, 161 (2016).
6. P. Loiko, L. Zhang, J. M. Serres, Y. Wang, M. Aguiló, F. Díaz, Z. Lin, H. Lin, G. Zhang, E. Vilejshikova, E. Dunina, A. Kornienko, L. Fomicheva, V. Petrov, U. Griebner, W. Chen, and X. Mateos, J. Alloys Compd. **763**, 581 (2018).
7. Y. Wang, G. Xie, X. Xu, J. Di, Z. Qin, S. Suomalainen, M. Guina, A. Härkönen, A. Agnesi, U. Griebner, X. Mateos, P. Loiko, and V. Petrov, Opt. Mater. Express **6**, 131 (2016).
8. K. van Dalfsen, S. Aravazhi, C. Grivas, S. M. García-Blanco, and M. Pollnau, Opt. Lett. **39**, 4380 (2014).
9. A. G. Okhrimchuk and P. A. Obraztsov, Sci. Rep. **5**, 11172 (2015).
10. F. Chen and J. R. Vázquez de Aldana, Laser Photon. Rev. **8**, 251 (2014).
11. D. G. Lancaster, S. Gross, A. Fuerbach, H. E. Heidepriem, T. M. Monro, and M. J. Withford, Opt. Express **20**, 27503 (2012).
12. E. Kifle, P. Loiko, J. R. V. de Aldana, C. Romero, A. Ródenas, S. Y. Choi, J. E. Bae, F. Rotermund, V. Zakharov, A. Veniaminov, M. Aguiló, F. Díaz, U. Griebner, V. Petrov, and X. Mateos, Photon. Res. **6**, 971 (2018).
13. L. Zhang, H. Lin, G. Zhang, X. Mateos, J. M. Serres, M. Aguiló, F. Díaz, U. Griebner, V. Petrov, Y. Wang, P. Loiko, E. Vilejshikova, K. Yumashev, Z. Lin, and W. Chen, Opt. Express **25**, 3682 (2017).
14. A. Ródenas, A. H. Nejadmalayeri, D. Jaque, and P. Herman, Opt. Express **16**, 13979 (2008).
15. J. A. Caird, S. A. Payne, P. R. Staber, A. J. Ramponi, L. L. Chase, and W. F. Krupke, IEEE J. Quantum Electron. **24**, 1077 (1988).
16. K. van Dalfsen, S. Aravazhi, D. Geskus, K. Wörhoff, and M. Pollnau, Opt. Express **19**, 5277 (2011).
17. P. Loiko, X. Mateos, S. Y. Choi, F. Rotermund, J. M. Serres, M. Aguiló, F. Díaz, K. Yumashev, U. Griebner, and V. Petrov, J. Opt. Soc. Am. B. **33**, D19 (2016).
18. J. I. Mackenzie, S. C. Mitchell, R. J. Beach, H. E. Meissner, and D. P. Shepherd, Electron. Lett. **37**, 898 (2001).